

Modularized, Reconfigurable and Bidirectional Charging Infrastructure for Electric Vehicles with Silicon Carbide Power Electronics (MoReSiC)

Deliverable D.5.1 (Month 22)

Title: “Developed converter control algorithm capable of operation in all modes and with supplementary DC link (+/-750V) voltage balancing implemented in digital control system.”

Authors:

Radosław Sobieski, Markel,
Rafał Kopacz, Warsaw University of Technology.



Executive summary

The deliverable includes the control algorithm capable of operation in all modes and with supplementary DC link voltage balancing implemented in the digital control system, developed for the non-isolated DC/DC converter operating as the battery interface in the MoReSiC system. Additionally, this report also concerns an initial experimental prototype, built for the preliminary testing of the control algorithm. The deliverable was performed by the joint work of the team from Warsaw University of Technology and the Markel employees. After the initial analysis, the three-level synchronous topology was selected, also including the submodule developed in the frame of WP2 as the base for the DC/DC converter. At first, a series of simulations were performed in PLECS, to analyse the possible inductor configurations, and the different modulation strategies, as well as their impact on the rest of the converters. Furthermore, control loops for both DC-link voltage balancing, as well as inductor current levelling were also developed. Then, to transfer the control system from software to hardware, an initial prototype was constructed. Finally, the control algorithm was applied to a suitable DSP-based system, and validated in preliminary experimental tests.

Table of Contents

- 1. Topology selection for the non-isolated DC/DC converter.....3**
- 2. Inductor configurations, modulation strategies & control5**
- 3. Simulation study.....10**
- 4. Initial experimental prototype of the converter.....13**
- 5. Hardware validation of the control system15**
- 6. Summary.....16**

1. Topology selection for the non-isolated DC/DC converter

The research in WP5 started with the selection of a proper topology for the non-isolated DC/DC battery converter under the first task: T5.1 *Assessment of the fundamental design of a non-isolated DC/DC converter topology enabling bidirectional operation and three-level voltage on the high side*. The critical function of this power electronics system is to interface the power flow from the three-wire DC-link (+750/0/-750V) in the charging station and the battery energy storage system rated at 800 V nominal voltage, assuming the energy flow in both directions (from and to the battery energy storage). Furthermore, it is required that the converter is capable of balancing the voltages of the three-wire DC-link, in case of operation without the AC/DC converter turned-on. Finally, since the converter was developed in the frame of the MoReSiC system, the converter had to be designed using 1.2 kV SiC power devices, and the three-level power submodules developed within the other part of the project (WP2).

On the basis of prior work in other work packages, especially WP3, some potentially prominent topologies such as the Flying Capacitor Converter (FCC), T-type converter, were decisively dismissed as in these topologies there is no connection to the 0 V potential in the three-wire DC-link structure, thus, making it impossible to balance the voltage between the DC-link capacitors. Furthermore, derivating from the ANPC topology chosen for the grid converter, and only using four transistors per leg, a well-known three-level DC/DC converter structure, also referred as double synchronous converter, can be established, as shown on the example of a single leg in Fig. 1. This topology is very straightforward, has a low component count and is capable of reaching high efficiencies, as well as meets all the requirements sourced in the MoReSiC system and described above. To be more thorough, in order to use the ANPC submodules, only a minor change has to be made – the additional two transistors have to be omitted and two paths have to be shorted. Thus, the submodule can be easily used in this system without any changes to the PCB scheme established before.

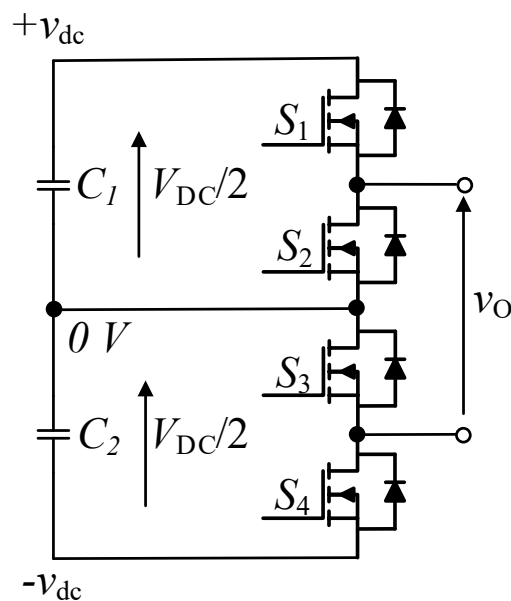


Fig. 1 One leg of the three-level DC/DC converter.

However, to meet the expected power rating (20 kW) and fully comply with the rest of the charging system, most importantly with the submodule from WP2 capable of transferring maximally 10 kW, at least two submodule units had to be employed. Furthermore, lowering the output ripples of the converter is especially important for battery-oriented systems, as in this case. Thus, an interleaved structure is recommended. Here, a two-phase system is initially chosen, as for the considered battery system with 800 V nominal voltage, operating points near $D=0.5$ result in the lowest ripples (DC supply at 1500 V).

The whole DC/DC converter in the chosen three-level topology, on the example of a buck configuration, is depicted in Fig. 2. Here, apart from the two legs built from the submodules, an output capacitor for lowering the output voltage ripples has to be added, along with a group of inductors, here shown in the most straightforward configuration (four non-coupled inductors).

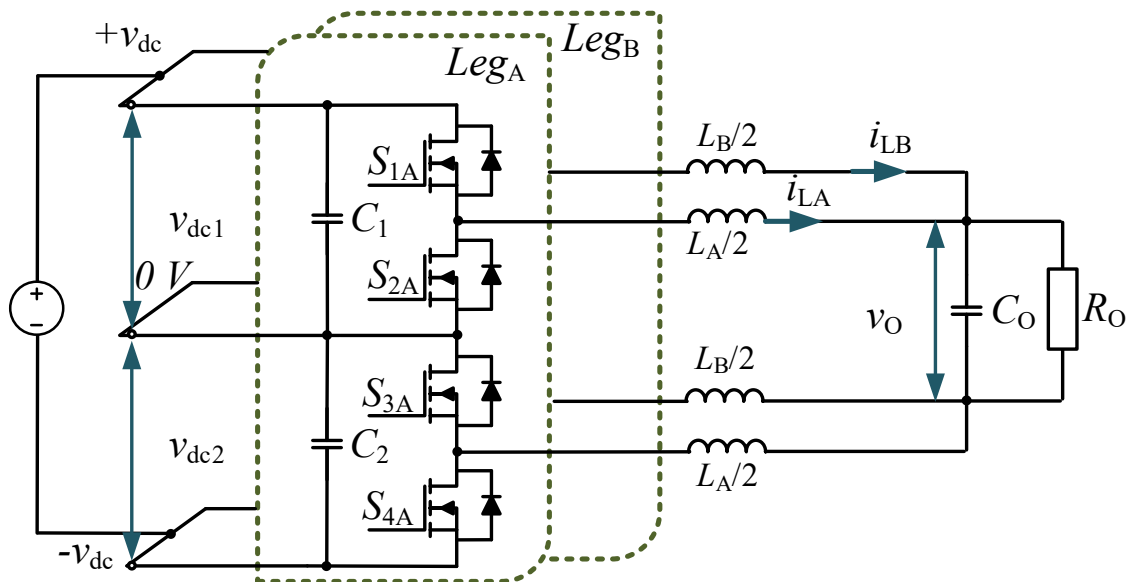


Fig. 2 The chosen topology of the DC/DC converter (in exemplary buck configuration).

2. Inductor configurations, modulation strategies & control

While the basic topology of the three-level DC/DC converter is straightforward in terms of the leg structure, the possible modulation strategies, and the different applicable inductor configurations render the system more complex. Considering this options is essential to establish an optimized system for a specific application, such as a non-isolated DC/DC converter operating as a battery interface in a bipolar fast charging station system, and prepare the control scheme. This section is directly associated with task T5.2 *Theoretical and simulation-based verification of various configurations of the non-isolated DC/DC converters for supplying charging power in the range of 10-20 kW*, as the theoretical analysis is considered here, while the simulation verification is described in the next section.

At first, the possible inductor configurations were analysed. Based on a thorough literature review, prior experiences of the team, and new ideas, three possible solutions were found, as shown in Fig. 3. The first approach, depicted in Fig. 3a, is the most conventional – to use four separate non-coupled inductors (4sI). This method is very straightforward. The construction of the magnetic components is the simplest, and in accordance with the analysis described in the next section all modulation strategies are applicable.. However, since four single inductors are used, the volume of the magnetics is notable, specifically when compared to other more sophisticated solutions with coupled inductors.

Using coupled inductors is a well-known technique, to limit the total volume, as instead of using four cores, only 2 are required. Furthermore, with proper orientation of the flux within the magnetics, the inductor ripples can be also minimized. Here, two possible configurations were found. Fig. 2b presents the state-of-the-art topology from the literature, with two common-potential coupled inductors (2cI-P). In this configuration, the coupled inductor is connected based on the potential of the converter legs – in one inductor it is the positive potential (terminal A+ and B+), and in the other the negative one (A-, B-). In such a situation, when negative coupling is used the output ripples, especially important for battery-oriented applications, are lowered compared to the conventional solution (4sI). Here, also all modulation schemes are possible.

The final configuration also employs coupled inductors. However, in this case, the connection is different, as shown in Fig. 3c. The coupled inductors are connected in common-leg configuration (2cI-L), one inductor to terminals A+. A-, and the other to B+. B-. When a positive coupling is applied, this configurations also shows low output ripples, especially for duty near 0.5, which is the case of the battery DC/DC converter in the MoReSiC system. However, this configuration cannot be controlled with all the modulation strategies, which is elaborated on further in this report. Moreover, this idea is novel and has not yet been investigated in the literature.

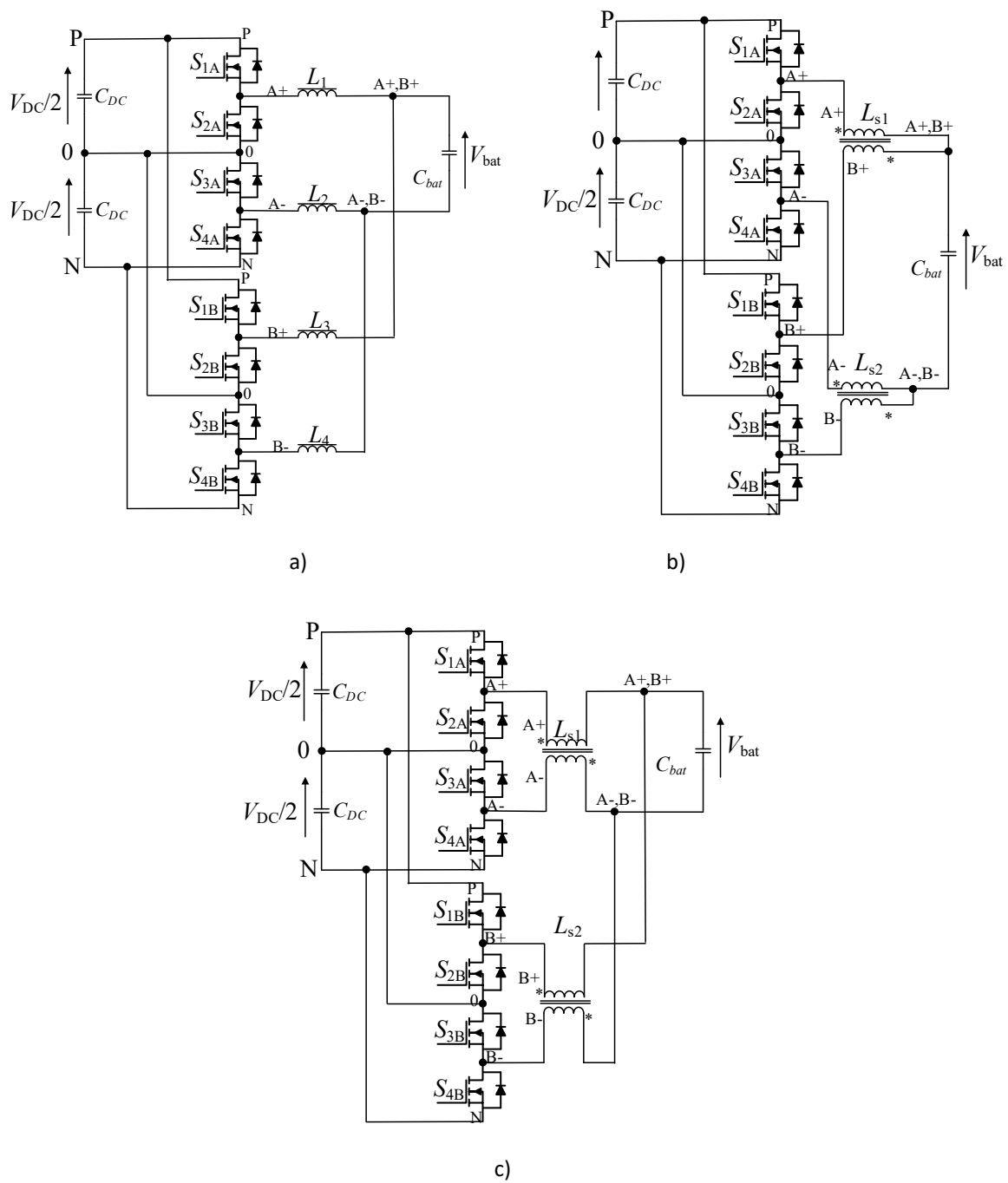


Fig. 3 Three possible inductor configurations for the DC/DC converter: a) four separate inductors (4sI), b) two common-potential coupled inductors (2cI-P), c) two common-leg coupled inductors (2cI-L).

Another crucial consideration regards the modulation technique. In the DC/DC converter of interest, four main modulation strategies can be named and are shown in Fig. 4. The first modulation, depicted in Fig. 1a, is the conventional non-interleaving modulation (referred as I-type), where the two legs are controlled with the same signals. Using this scheme, the system actually becomes equal to a single-phase non-interleaved system, and even a single inductor (with inductance equal to 4 times the inductance of each from the four separate inductors) can be used. Generally, using this modulation method, the multi-phase character of the system is not utilized, and thus the ripples are quite high. However, since the DC/DC converter has to be made employing at least two submodules (2 x 10 kW), it can be still applied. Furthermore, using this strategy, no current balancing techniques need to be employed.

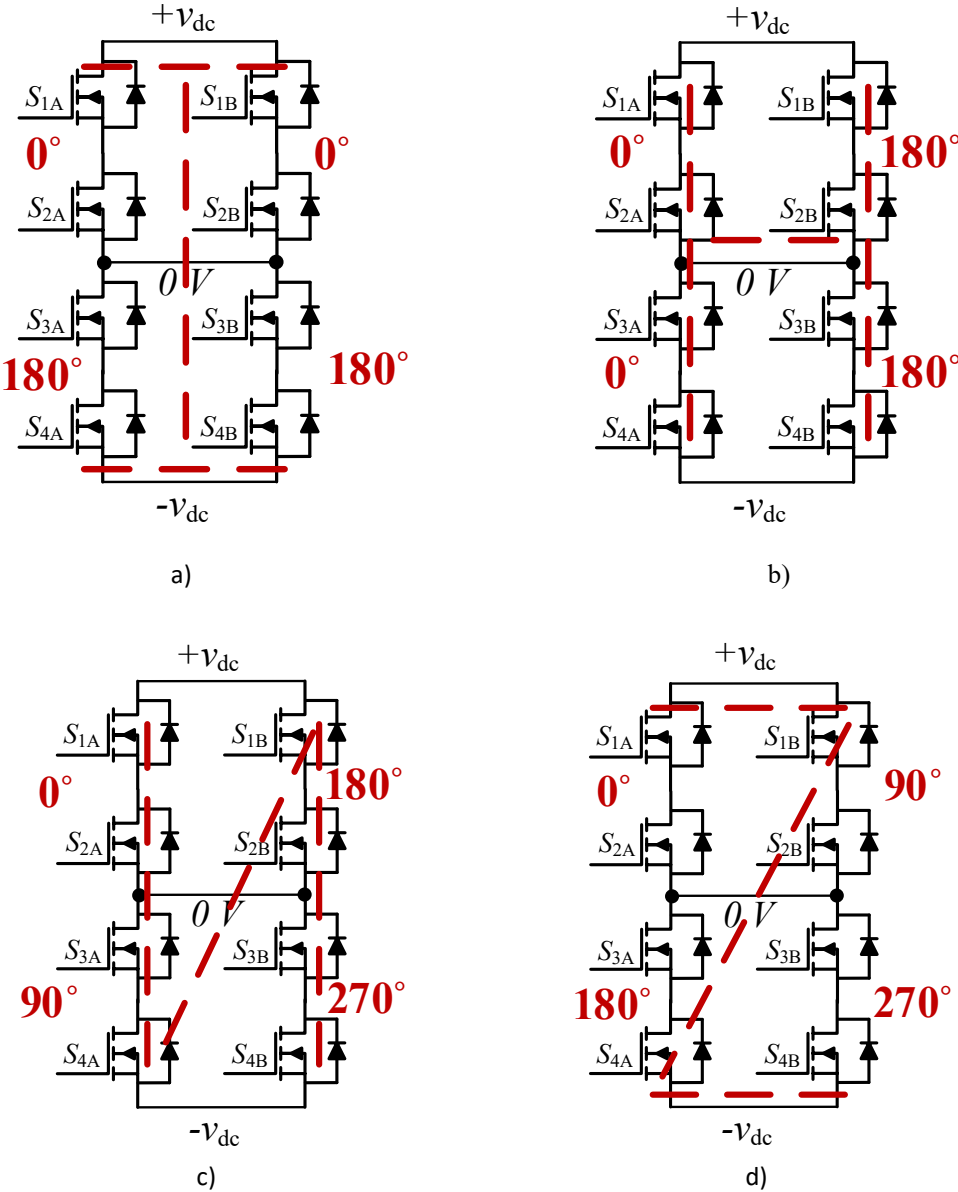


Fig. 4 Modulation strategies applicable in the DC/DC converter: a) conventional non-interleaving modulation (I), b) conventional interleaving modulation (H), c) N-type interleaving modulation (N), d) Z-type interleaving modulation (Z).

The second modulation technique, shown in Fig. 4b, is the conventional interleaving modulation (here referred as H-type). In this method, the two legs are shifted in phase by 180 degrees. Thus, the inductor currents cancel out, and the output ripples are minimized. This is the technique that can be effectively used in the 2cI-L configuration. The third modulation strategy is the N-type technique. Similarly, as for the other modulations, the name refers to the phase shifts in the transistor control signals, as depicted in Fig. 4c. Applying this technique, makes the output ripples even lower, however with a slight cost in the form of additional power losses. Finally, the Z-type technique presented in Fig. 4d is similar to the N-type in terms of output ripples. However, it is usually considered inferior to N-type in the literature, as it shows higher EMI.

Exemplary transistor control signals for the most complex strategy, the N-type modulation, with the expected inductor currents, along with the description of the basic switching states of the converter is shown in Fig. 5 and Tab. 1 respectively.

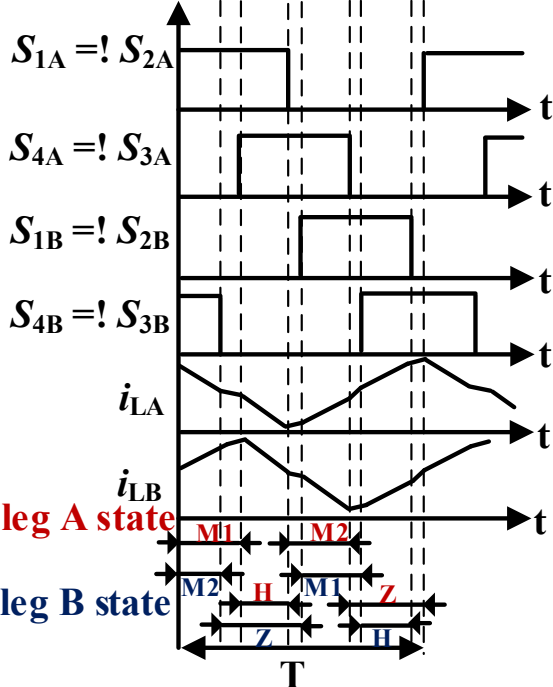


Fig. 5 Exemplary transistor control signal for the N-type modulation strategy.

Tab. I Basic switching states of the DC/DC converter in buck mode

State	S_1	S_2	S_3	S_4	Output voltage
High state (H)	1	0	0	1	V_{DC}
Medium state 1 (M1)	1	0	1	0	$V_{DC}/2$
Medium state 2 (M2)	0	1	0	1	$V_{DC}/2$
Zero state (Z)	0	1	1	0	0

Considering all the possible modulation strategies, along with the different inductor configurations, a control scheme was prepared for each of the methods. Thus, the many option could have been compared, both in simulations, as well as later on the experimental prototype. The proposed control system is shown in Fig. 6 on the example of buck mode operation, this converter with the control system is also applicable in boost mode with the opposite direction of power flow, as long as the voltage controller is driven by the grid-side DC voltage values, depicted as V_{dc} . Furthermore, in the Fig., the 4sI configuration is presented, however the method is universal for all configurations and modulation techniques.

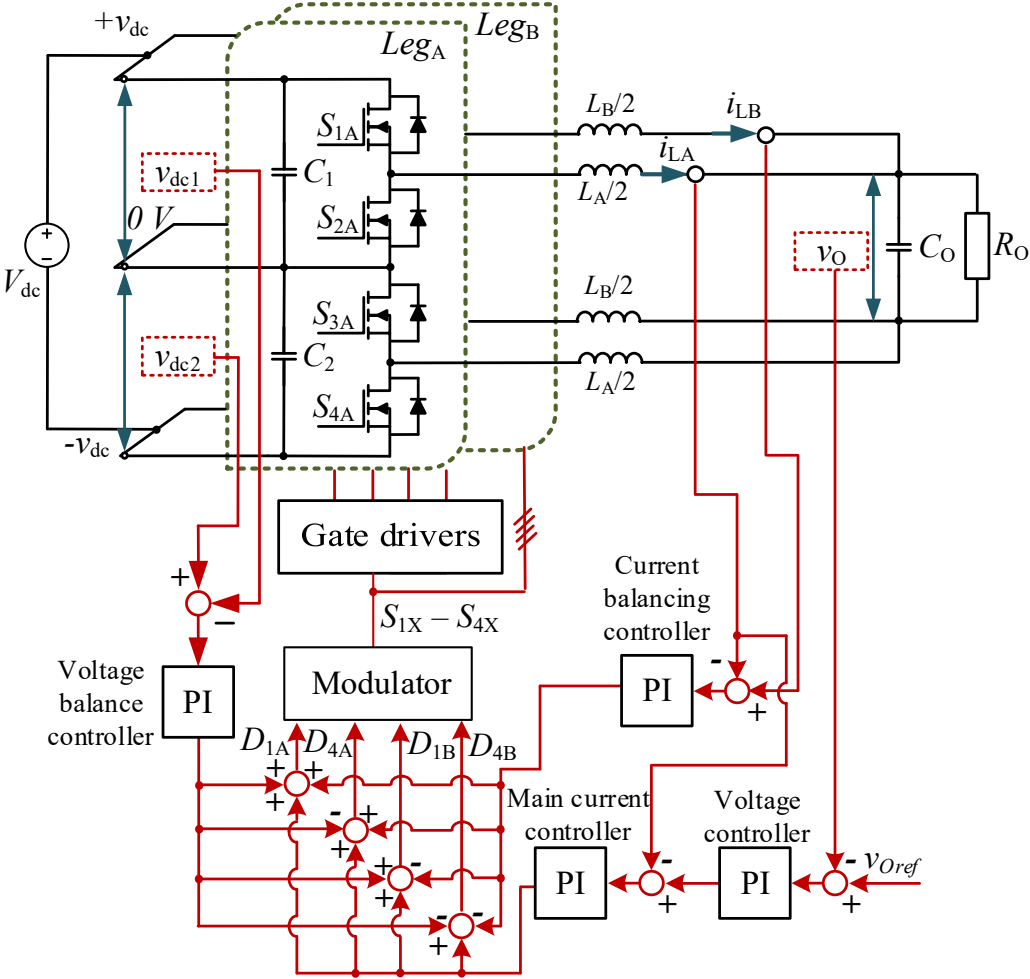


Fig. 6 Control scheme for the DC/DC converter, shown on the example of buck mode operation.

In the system, the core control path consists of a primary current PI (proportional-integral) controller and a secondary voltage controller, where the reference value of the output voltage is given. Using the output of the main current control, the dominant part of duty cycles D_A (for leg A) and D_B (for leg B) are calculated and used to drive the converter.

However, additional balancing measures are required for the proper operation of the converter. Firstly, the 3-pole DC bus connection necessitates levelling the DC voltages at capacitors C_1 and C_2 . Based on an error value from the difference between the measured v_{dc1} and v_{dc2} voltages, a voltage-balancing PI controller regulates the duty cycles of the converter. The output of the controller is either added (for signal $S4=!S3$) or subtracted (in the case of

signal $S1=!\!S2$) to the duty cycle value. Therefore, such an approach allows for voltage balancing without affecting the output voltage.

Furthermore, balancing currents between the interleaved legs is also a necessity in most of the modulation techniques to limit the currents circulating in the inductors and minimize additional power losses. This can be achieved through two separate control paths consisting of a voltage and a current controller for each leg. However, using this method, the total count of controllers is five. Thus, in the presented system, to limit the number of regulators, another approach was assumed. The core control path (voltage and main current controllers) is used to set the duty cycles for both legs, and an additional current controller using the difference between the inductor currents i_{LA} and i_{LB} as an error is used. Therefore, the output from the current balancing controller is added to D_A value and subtracted from D_B , and similarly, as in the voltage balancing controller, the output is unaffected. Moreover, apart from lowering the number of total regulators to four, the current balancing controller is less susceptible to noise, as the error uses two measured values as an input, and therefore the interferences cancel out.

All in all, the proposed control diagram fulfils all requirements issued by the MoReSiC charging system, including voltage and current balancing, as well as bidirectional operation, and could have been used in further analyses, both in simulations and experiments, as well as in the final converter (deliverable D.5.2). Thus, task T5.3 *Development of the DC/DC converter control algorithm including DC voltage balancing system and operation at maximum efficiency in different operation modes* was completed.

3. Simulation study

The next step was to develop simulation models and perform the simulation study to finish tasks T5.2 *Theoretical and simulation-based verification of various configurations of the non-isolated DC/DC converters for supplying charging power in the range of 10-20 kW*, and also T5.4 *Identification of electrical and thermal operating parameters in terms of voltage, current and temperature*. Similarly, as in the other work packages, PLECS software from Plexim was used, as it provides the possibility to simulate both the control and operation of the converter, as well as to help with the power loss estimation required for identification of the electrical and thermal operating parameters for the design of the experimental model, both for WP2 and WP5.

The results from the exemplary simulation performed in the steady-state are showcased in Fig. 7 and 8. Please note, that here only results for inductor configuration 4sI and N-type modulation are shown, while other configurations also were tested. The results from the study at nominal operating point at 1500 V input, 800 V output, and 20 kW power is depicted in Fig. 7, while another point, directly correlating with the exemplary experimental test shown further in the report, performed at 800 V input, 590 V output, and power of 10 kW is shown in Fig. 8. As can be observed, the control system operates as assumed: the output voltage is steady at the reference value, the DC bus voltages are well-balanced with minimal ripples, and the inductor currents are levelled as well. Moreover, even though the momentary currents of individual inductors are high, due to the interleaved structure and N-type modulation, the ripple of the sum inductor current is at low levels, at roughly 5% of the nominal value. Therefore, ripples of both output current and voltage are minuscule. However, it is worth noting that in a real-life application, the connections, e.g., cables, to the battery energy storage system can be lengthy,

and thus extra parasitic inductance appears, causing the output ripples to increase radically. Moreover, it can be seen that using the N-type modulation, the current shape is either triangular (for duty near 0.5), or closer to a trapezoidal shape. All in all, the simulations prove that the DC/DC converter can adequately operate with the presented control system.

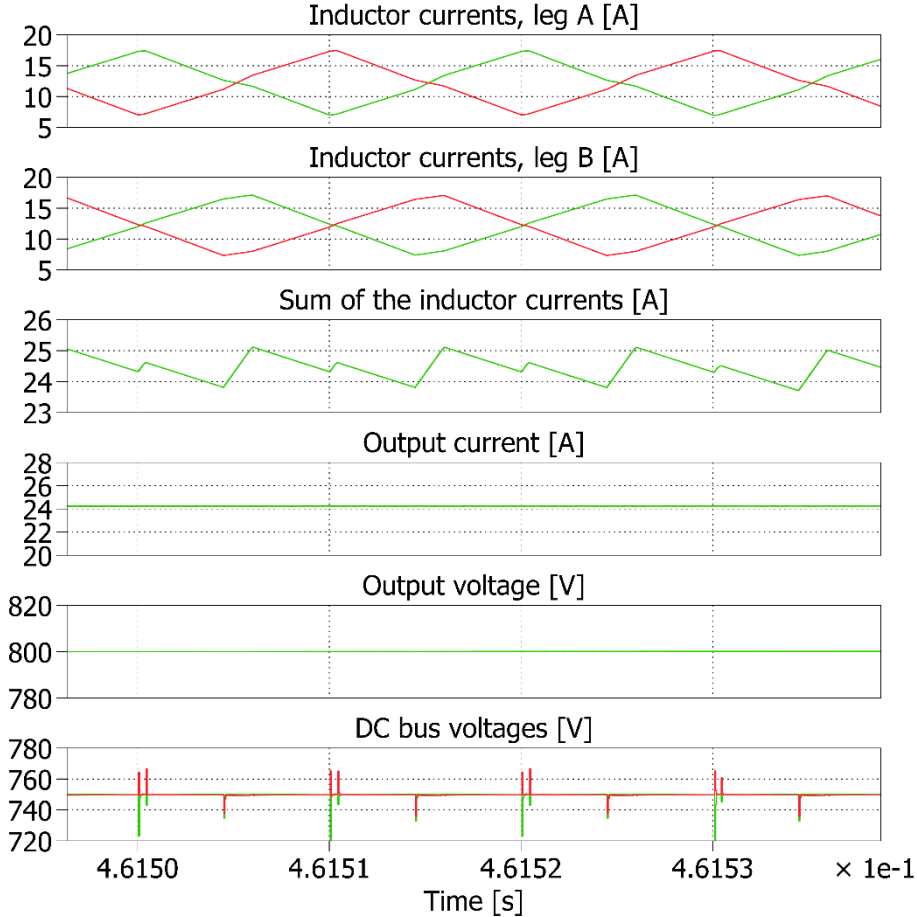


Fig. 7 Exemplary simulation results of the DC/DC converter – case 1, 1500 V input, 800 V output, 20 kW power.

Finally, the last part of the simulation study regarded the establishing the electrical and thermal operating parameters for the design of the experimental model. Thus, a power loss-oriented study was conducted, for different types of transistors, number of interleaved legs (2 or 3). Based on the results from this research (depicted in Fig. 9, and a similar study made for the grid converter, the NTH4L040N120SC1 transistor were chosen as the most efficient ones compared to other state-of-the-art and available 1200 V-rated SiC MOSFETs, thus completing task T5.4 *Identification of electrical and thermal operating parameters in terms of voltage, current and temperature.*

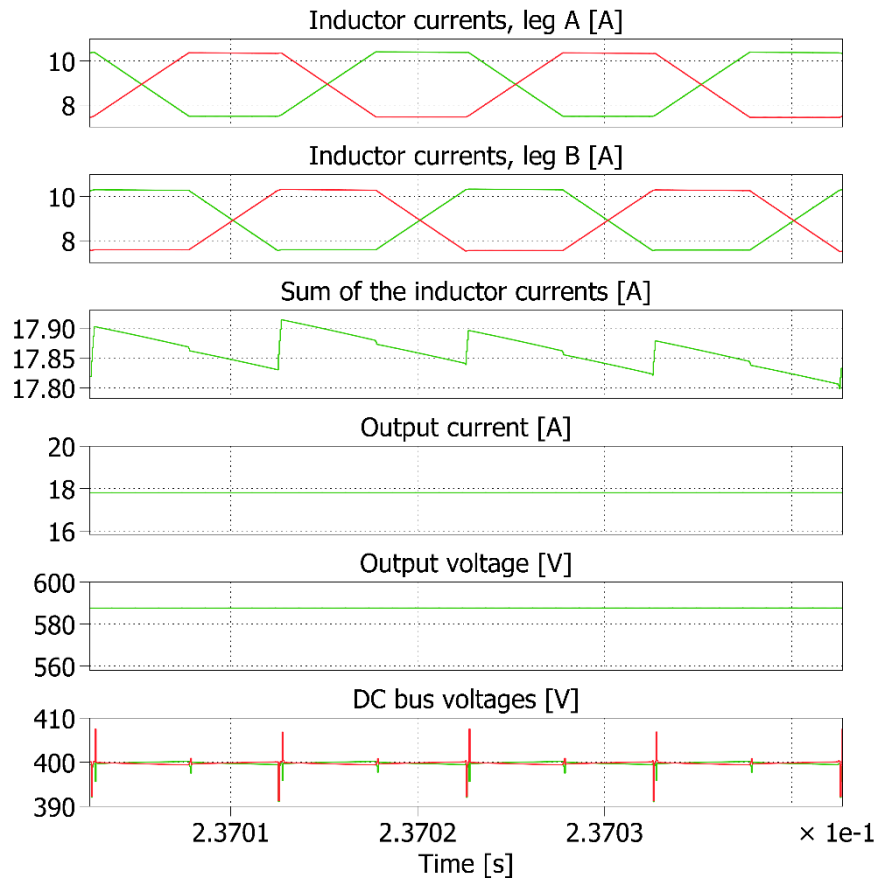


Fig. 8 Exemplary Simulation results of the DC/DC converter – case 2, 800 V input, 590 V output, 10 kW power..

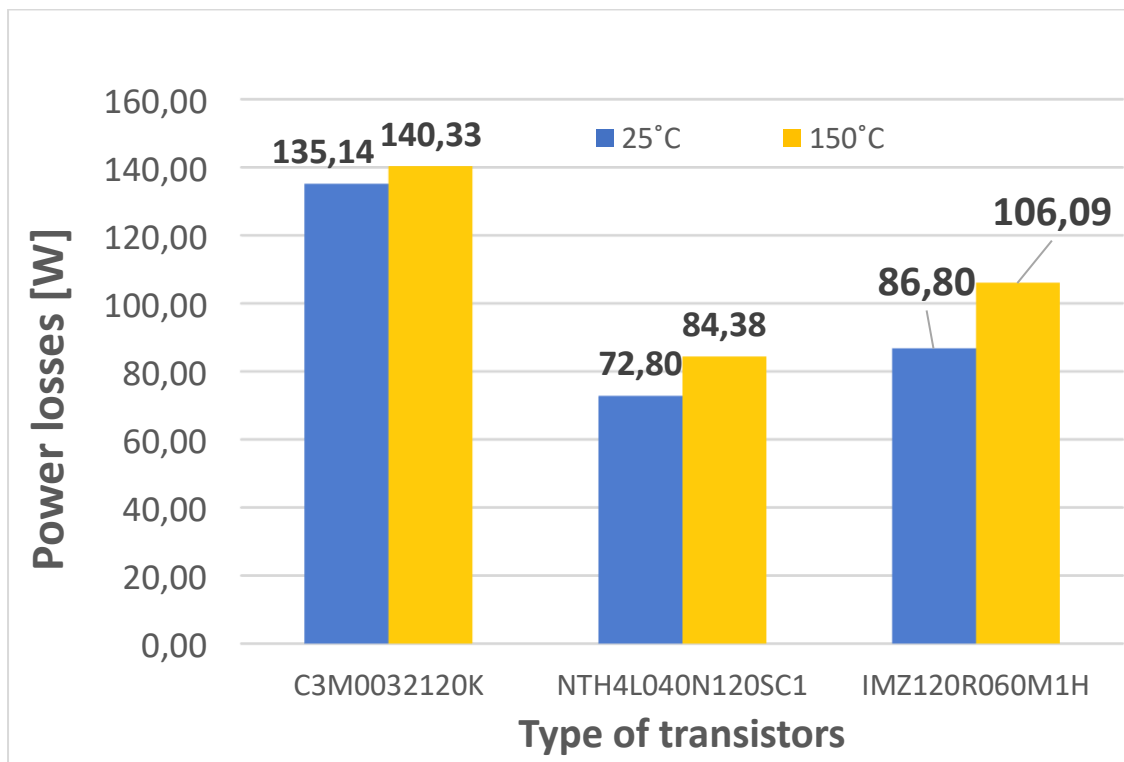


Fig. 9 Simulation-based assessment of power losses for different state-of-the-art SiC MOSFETs.

4. Initial experimental prototype of the converter

In order to validate the control scheme of the DC/DC converter, an early experimental prototype was designed and constructed. Thus, work on task T5.5 *Design of the non-isolated DC/DC converter including main circuit layout with the necessary auxiliary sub-circuits and high-frequency magnetic components* has already started. To expedite the process, an available control board constructed earlier in other projects at WUT was used. Moreover, because of the problems with availability of the components, also the measurement circuits for the voltages and currents were based on systems developed for other converters. While these solutions were not ideal for the DC/DC battery converter, they were sufficient to test the control method and validate it, while the final version would have a dedicated system, both for the DSP control, as well as the measurement and conditioning systems.

The basic parameters of the DC/DC converter early prototype are the same as will be for the final version, and are presented in Tab. II. The DC-link voltage is 1500 V (750 + 750), while the nominal output (battery) voltage is 800 V. In order to limit the power losses and omit potential issues in communicating the DC/DC converter with the grid ANPC converter, the frequency was set to 62.5 kHz. Furthermore, the inductor values were calculated as roughly 620 μ H total, with 60 μ F output capacitance to reach output ripples below 2%. Please note, that four inductors in 4sI configuration are shown in the prototype, as the basic, conventional solution. However, other configurations have also been tested with different inductors connected, and other modulations applied. Finally, the system uses two power submodules from WP2, shown in Fig. 10, with four transistors per each leg.

Tab. II Basic parameters of the 20 kW DC/DC converter

Nominal battery voltage	800 V
DC-link voltage $V_{dc1} + V_{dc2}$	1.5 kV
Switching frequency	62.5 kHz
Filter inductances L_A, L_B, L_C	4 x 155 μ H
Battery-side capacitance	60 μ F
DC-link capacitances	4 x 60 μ F
Power SiC transistors	8 x NTH4L040N120SC1
Number of submodules (WP2)	2

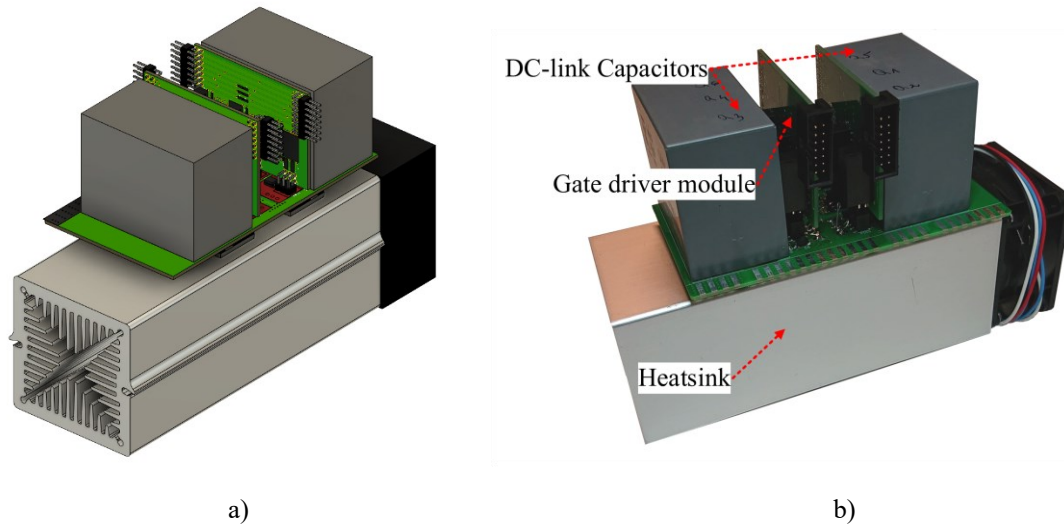


Fig. 10 The power submodule (WP2): a) 3D model, b) photo.

Apart from the power circuit, two submodules, and the inductors, the system was built using a control board based on TMS320f28379D digital signal processor, and a number of measurement circuits. Except for the core ones enumerated in the control section (two DC bus voltage measurements, output voltage measurement, and two inductor current meters), there are more measurements required for the full charging station operation. To be more specific, it is required to measure the power flow into and out of the converter. Thus, additional output current meter and two input current measurements were added (one per half of the DC bus). All the current meters were constructed using LEM transducers, LA-55 for the inductor currents and LAH-50 for the DC currents. The voltage measurements were based on self-made PCBs, using optocouplers and amplifiers to construct an isolated voltmeter system.

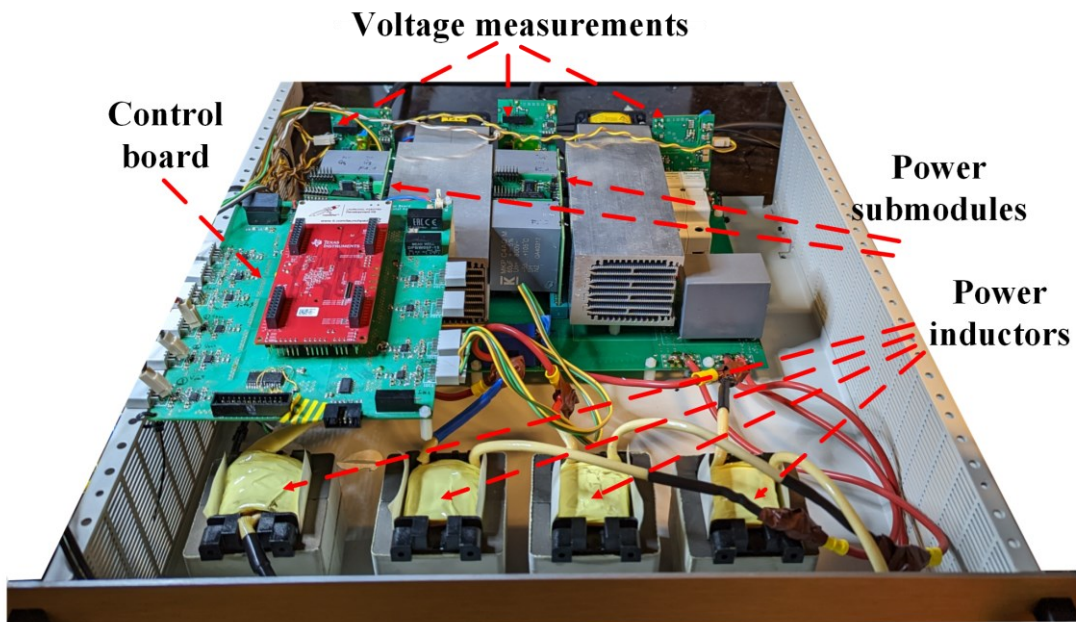
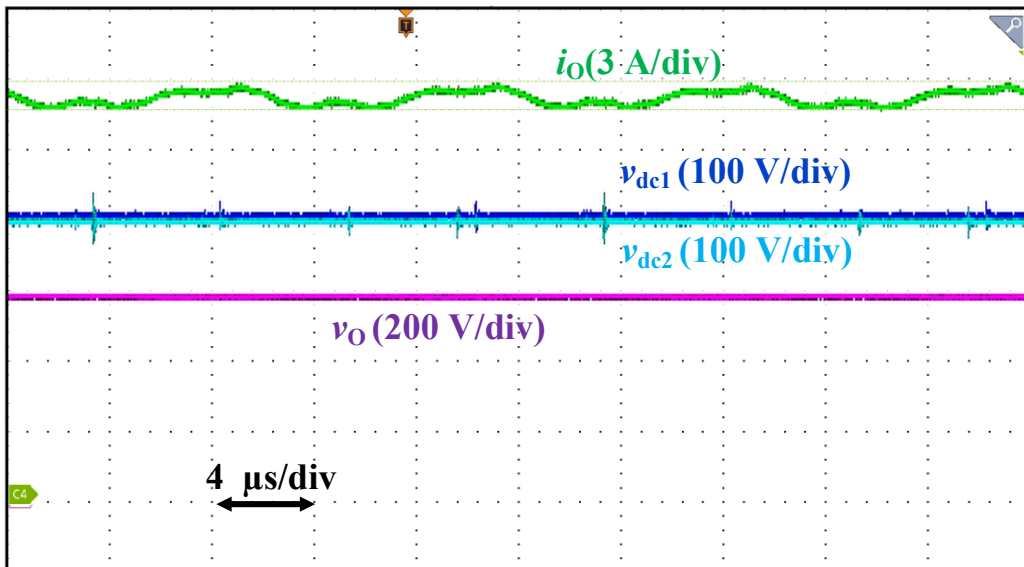


Fig. 11 Photo of the initial experimental prototype constructed for validation of the control algorithm.

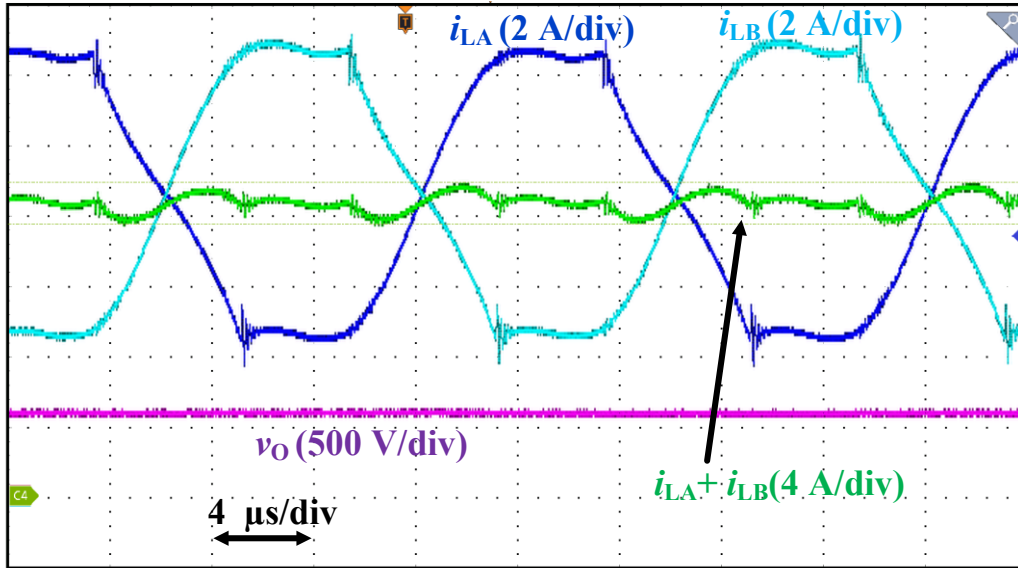
5. Hardware validation of the control system

Using the built converter prototype with the developed control method, a series of initial experimental tests, showcasing proper operation of the converter under the proposed control system, were performed. The results from the initial experiments are presented in Fig. 12, and depict the operation with N-type modulation, as well as 4sI inductor configuration. The exemplary test was performed at reduced power of 10 kW power, 800 V, and a load of 34 Ω , resulting in a voltage gain of roughly 0.74. Analyzing Fig. 12a, it can be seen that the DC-link voltages are well leveled using the presented voltage balancing method, with a difference below 1% of the nominal DC voltage (roughly 7 V) and some minor overshoots appearing at the time of transistor switching (at approximately 40 V). Therefore, the voltage among the transistors in the multilevel structure is balanced as well, providing safe operating conditions for the converter. Furthermore, the output current of the converter is characterized by very low ripples – 0.6 A, corresponding to less than 4% of the i_o steady-state value. This is crucial since the converter is designed to cooperate with a battery energy storage system. Finally, the output voltage is stable and reaches the reference value of 590 V.

Fig. 12b is focused on exhibiting the performance of the inductors. As can be observed, thanks to the current balancing regulator, the inductor currents are equal in terms of the mean value for both legs, limiting the possible circulating current described in the previous sections. Moreover, even though the momentary current ripples of the individual inductors are on a significant level (with peak-to-peak currents at roughly 9.3 A compared to a maximum value of 12.5 A), by applying the N-type interleaving method, the sum inductor current flowing to the output capacitor is steady, with current ripples at approximately 8% of the nominal mean value (16.7 A).



a)



b)

Fig. 12 Results from the initial experimental test, performed at 800 V DC voltage, 10 kW power and a load of 34 Ω , voltage gain of roughly 0.74: a) general view with output current and voltage, as well as the DC bus-side voltages; b) inductors-focused view with i_{LA} , i_{LB} , and sum inductor current of the positive output pole $i_{LA} + i_{LB}$.

In fact, it has been validated that the DC/DC converter prototype under the developed control method behaves as anticipated, with balanced DC-link voltages and inductor currents and low output ripples. Thus, it can be effectively applied in a bipolar grid-based EV charging station and further applied to the final, optimized prototype under deliverable D.5.2, and later finish task T5.6 *Delivery and initial tests of the non-isolated DC/DC converter in all operation modes*.

6. Summary

The developed control method for the DC/DC battery converter to be applied in the MoReSiC system was successfully proposed and validated, both in simulations, as well as through initial experimental tests using a very early prototype. The applied control method fulfils all the requirements, the converter reaches the set reference values using both voltage and current control, as well as is capable of balancing the DC-link voltages when needed, while maintaining levelled inductor currents. Thus, the control system can be successfully used in the final prototype of the converter. Even though an early prototype have been already built and initially tested, further works leading to completion of deliverable D.5.2 will include a more advanced, optimized version of the converter, as well as full experimental study regarding the required operation, including tests rated at 20 kW, in both directions. In summary, the assumptions regarding the milestone have been achieved. Apart from the work on the D.5.2, also additional research is planned on experimental study on the different inductor configurations, including the novel 2-cI-L topology.